

# Deep Learning of Diffuse Optical Tomography based on Time-Domain Radiative Transfer Equation

Yu-ichi Takamizu<sup>1</sup>, Masayuki Umemura<sup>1</sup>, Hidenobu Yajima<sup>1</sup>, Makito Abe<sup>1</sup>, and Yoko Hoshi<sup>2</sup>

<sup>1</sup> Center for Computational Sciences, University of Tsukuba, 1-1-1 Tennoudai, Tsukuba-shi Ibaragi Japan

<sup>2</sup> Preeminent Medical Photonics Education and Research Center, Hamamatsu University School of Medicine, 1-20-1 Handayama, Higashi-ku Hamamatsu, Sizuoka Japan  
[takamizu@ccs.tsukuba.ac.jp](mailto:takamizu@ccs.tsukuba.ac.jp)

**Abstract:** Near infrared diffuse optical tomography (DOT) provides an imaging modality for the oxygenation of tissue. In this paper, we propose a novel machine learning algorithm based on time-domain radiative transfer equation. We use temporal profiles of absorption measure for a two-dimensional model of target tissue, which are calculated by solving time-domain radiative transfer equation. Applying a long-short-term memory (LSTM) deep learning method, we find that we can specify positions of cancer cells with high accuracy rates. We demonstrate that the present algorithm can also predict multiple or extended cancer cells.

© 2022 Optical Society of America

## 1. Introduction

Diffuse optical tomography (DOT) using near infrared light (700 nm- 900 nm) is one of the most sophisticated optical imaging techniques for biological tissue. Especially, DOT can provide a promising imaging modality for cancer detection owing to its contrast to hemoglobin oxygenation level. To reconstruct optical properties of tissue in DOT, two mathematical problems should be solved, i.e., the forward and the inverse problem [1]. The forward problem is to pursue the propagation of scattered light in biological tissue and thereby predict the scattered light measurements for a setup of tissue optical properties, while the inverse problem is to reconstruct tissue optical properties from scattered light measurements by use of the forward model. The image reconstruction in DOT is a nonlinear ill-posed inverse problem, which is subject to the shortage of data diversity and instabilities to noise. Hence, the feasibility of DOT depends upon how precisely the forward problem is calculated and how stably the inverse problem is solved.

The propagation of light with scattering and absorption is rigorously governed by the radiative transfer equation (RTE) [2]. Numerical schemes to directly solve RTE in biological tissue have been proposed [3, 4]. However, they are computationally expensive, since RTE in three-dimensional space results in a six-dimensional problem in a photon phase space. Also, to converge the inverse problem, the forward problem should be solved several times for a single reconstruction. Hence, the RTE calculations have been an unavoidable bottleneck in algorithms to solve the inverse problem. So far, light propagation has been often approximated by a diffusion equation (DE) using the P1 approximation of the RTE. The diffusion approximation is

a simplification of the RTE for optically thick media in which multiple scattering is dominant [5]. Based on frequency-domain as well as time-domain DE, various approaches for image reconstruction in DOT have been attempted [6, 7].

However, actual tissue systems follow the so-called mesoscopic scattering regime, where light undergoes multiple scattering but the scattered light is not perfectly diffusive. For mesoscopic scattering, the diffusion approximation breaks down especially near sources and boundaries. To circumvent the shortage of diffusion approximation, hybrid schemes that combine radiative transfer with diffusion have been implemented [8, 9, 10]. Hybrid schemes can reduce dramatically the computational cost to solve light propagation, but the boundaries between RTE and DE cannot be determined *a priori*. Therefore, overall RTE calculations are desirable. As for frequency-domain RTE, several solvers of the inverse problem have been proposed [11, 12]. However, image reconstructions based on time-domain RTE are still immature. The time-domain RTE provides more functional information on biological tissue.

Recently, machine-learning has brought a new possibility for image reconstructions. Actually, a deep learning scheme based on DE has been launched [13]. In this paper, we construct a novel machine learning algorithm based on time-domain RTE. In this algorithm, training data are the temporal profiles of light propagation in models mimicking biological tissue. For the purpose, we have developed a time-domain RTE solver, TRINITY (Time-dependent Radiation Transfer in Near-infrared Tomography), which is based on our former steady-state RTE solver, ART [14]. As for machine learning, we utilize an LSTM (Long Short-Term Memory) method, which is an extension of artificial recurrent neural network (RNN) architecture to process not only single data points but also entire sequences of temporal data.

## 2. Methodology

### 2.1. Model

Throughout this paper, we set up a two-dimensional model. We suppose target tissue with the size of  $4\text{cm} \times 4\text{cm}$ , in which we allocate 28 domains to specify the positions of cancer cells, as shown in Fig. 1. We assume a round absorber with diameter 5mm as a model of a cancer cell. This setup is based on the experiment using a phantom composed of polyoxymethylene. The optical properties of the phantom are characterized by

$$\mu_a = 0.21/\text{cm}, \mu_s = 22.45/\text{cm} \quad (1)$$

where  $\mu_a$  and  $\mu_s$  are the absorption and scattering coefficient, respectively. Within this background material, an absorbing pole with following coefficients

$$\mu_a = 0.64/\text{cm}, \mu_s = 22.63/\text{cm}, \quad (2)$$

is inserted. Scattering dominates absorption in the inserted pole as well as the background, but the absorption coefficient is larger by a factor of three in the pole. Therefore, absorption features due to the pole emerge in outgoing light at the boundary. That is a principle for detecting cancer positions in biological tissue. The incident beams and detectors are located at eight points as shown in the Fig. 1, where the positions of incident beams are labelled with S1-S8 and positions of detectors are with D1-D8.

We solve the following radiative transfer equation in two-dimensional space to pursue scattered and absorbed light,

$$\frac{1}{c} \frac{\partial I}{\partial t} + n \cdot \nabla I = -\mu I + \eta, \quad (3)$$

with

$$\mu = \mu_a + \mu_s, \eta = \mu_s \oint \phi(n, n') I(n') d\Omega', \quad (4)$$

where  $I$  is the specific intensity of light,  $\eta$  is the emissivity by scattered photons, and  $\phi$  is a phase function. The emissivity term represents radiative transfer from one direction  $n'$  to another direction  $n$ . We employ the Henyey-Greenstein function for  $\phi$ , that is,

$$\phi(n, n') = \frac{1}{2\pi} \frac{1 - g^2}{1 + g^2 - 2g(n \cdot n')}, \quad (5)$$

where  $g$  is the scattering anisotropy parameter. The case of  $g = 1$  or  $g = 0$  means perfectly forward scattering and isotropic scattering, respectively. We take  $g = 0.62$  for the phantom.

To solve Eq. (3), we have developed a new solver, TRINITY (Time-dependent Radiation Transfer in Near-infrared Tomography)(Yajima et al. in prep), which is based on our former steady-state RTE solver, ART (Authentic Radiative Transfer) [14]. This method is based on an idea that light ray is designed independently of spatial grids. The significant advantage is simultaneous reduction of computational cost and numerical diffusion. We set up  $64^2$  grids for radiative transfer calculations.

Using radiative transfer calculations, we define absorption measure as

$$A(t) = I_{\text{abs}}(t)/I_{\text{noabs}}(t) - 1, \quad (6)$$

where  $I_{\text{noabs}}$  is the intensity of outgoing light toward a detector when no absorber is settled, while  $I_{\text{abs}}$  is the intensity when one or multiple absorbers are embedded. The temporal profiles of  $A(t)$  provide training data in the LSTM machine learning. For an incident laser beam, we obtain datasets for temporal profiles of  $A(t)$  at the positions of 8 detectors.

Here, we consider the case for a laser beam injected from S2. Fig. 2 shows the resultant temporal profiles of absorption measure  $A(t)$ , depending on the position of absorber. For example, the upper left panel shows temporal profiles of  $A(t)$  for a absorber at #3. Since the absorber is very close to detector D8, a curve labeled with D8 shows significant absorption. Similarly, the lower left panel (absorber at #0) and the upper right panel (absorber at #26) exhibit strong absorption on the detectors in the vicinity of absorber. Lower right panel (absorber at #13) shows the result for absorber near the center of the whole region. In this case, all detectors recognize significant absorption, and also temporal profiles depend upon the detector position. These features of absorption measure  $A(t)$  are used for training data in the present deep learning.

## 2.2. LSTM deep learning method

In order to classify absorber positions, we employ a deep learning method. Deep learning based on artificial neural networks is one of powerful machine learning methods. Especially for temporal data, Long Short Term Memory (LSTM) learning is an effective tool that is an extension of artificial recurrent neural network (RNN) architecture to analyze not only single data points but also entire sequences of temporal data. LSTM networks have improved recurrent neural network by using the gates to selectively retain and forget information, which are relevant and not relevant, respectively. Lower sensitivity to time gaps makes LSTM networks robust for analysis of temporal data than a simple recurrent network.

We conduct deep learning based on two LSTM layers plus final Dense layer by using Tensor flow, which is an open platform for a machine learning provided by Google cooperation. In order to classify multiple domains, we use a categorical cross entropy for a loss function and a softmax activation function. The cross entropy loss function is defined as

$$-\sum_{c=1}^M y_c \log(p_c), \quad (7)$$

where  $M$  is the number of domains,  $y_c$  is a binary indicator which takes 1 if domain label  $c$  is the correct classification otherwise 0, and  $p_c$  is predicted probability observing domain  $c$ .

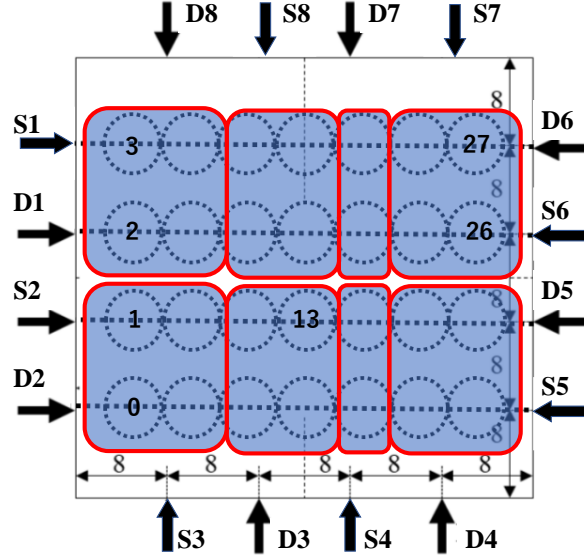


Fig. 1. The configuration of target tissue. The size is assumed to be 4cm  $\times$  4cm. There are located 28 domains, each of which can possess a round absorber with diameter 5mm. 8 incident beam directions (labelled S1-S8) and 8 detector positions (D1-D8) are shown. We divide the whole area into 8 groups, each of which has four or two domains.

We calculate a separate loss for each domain label and sum up over all domains. The softmax activation function is defined as

$$f_c(x_c) = \frac{e^{x_c}}{\sum_{i=1}^M e^{x_i}}, \quad (8)$$

where  $x_i$  is an element of input data vector  $\mathbf{x}$ . The softmax activation function is mainly used for a classification problem.

### 3. Multi-step classification method

It is difficult to classify all 28 positions directly at once. Thus, we make two-step classification. In the first step, all dataset are classified into 8 groups of domains, and each group is classified into domains in the second step. We find that such multi-classification method is useful for absorber detection. In Fig. 1, two-step classification is illustrated. The small box represents 8 groups and one group is composed of 4 or 2 domains.

The training and test data are the temporal profiles of absorption measure  $A$  at 8 detector positions, which are obtained by radiative transfer simulations for an absorber located at a domain. Moreover, we add random noises on simulation data. We attempt two types of noises. One is based on uniform random number in  $(0, 1)$  and its amplitude is assumed to be 0.01 in absorption measure  $A$ . The other is Gaussian noises, where random number produced by a Gaussian distribution function,  $\exp(-x^2/2\sigma^2)$  with a standard deviation  $\sigma$ . In the present analysis, we take  $\sigma = 0.001$ . This noise level is one tenth of uniform random noises, but it is suitable for classification by LSTM deep learning. Temporal profiles of absorption measure with noises are plotted in Fig. 3. We generate 2500 datasets in total, which include 89 datasets for each absorber position.

The first classification is constructed to determine learning parameters, where learning epochs are about 40 and the number of training data and test data is 2500 and 500, respec-

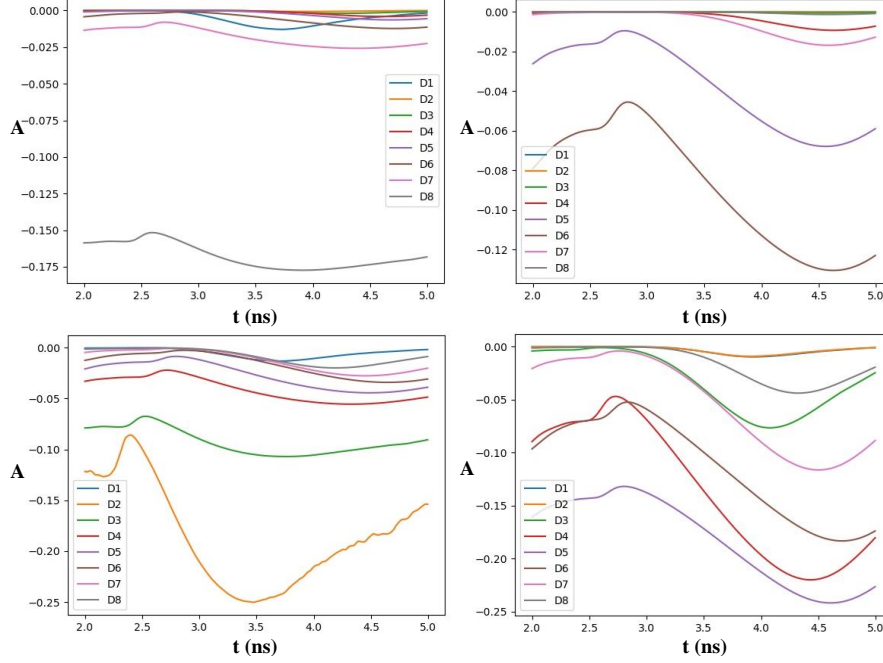


Fig. 2. Temporal profiles of absorption measure  $A = I_{\text{abs}}(t)/I_{\text{noabs}}(t) - 1$  on 8 detectors (D1-D8). The horizontal axis is time in units of nanoseconds (ns). Upper left panel shows the profiles for an absorber located at #3 position, upper right panel for an absorber at #26 position, lower left panel for an absorber at #0 position, and lower right panel for an absorber at #13 position.

tively. The final value loss is 0.03 and accuracy rate reaches 99% at the final epoch. The sub-classification in the second step is achieved more easily. For groups composed of 4 domains, learning epochs are 10 and the number of training data and test data is respectively 1000 and 200. For groups composed of 2 domains, learning epochs are 10 and the number of training data and test data is respectively 600 and 100. The final accuracy rate reaches 100% for such second-step classifications.

The constructed detection models can be tested using test data, which are generated by the same procedure for noise addition. First, we tried to test the detection model for uniform random noises. The resultant accuracy rate falls to 83%. It means that one always makes two mistakes to get two wrong positions within the total positions of 28. But, such discrepancy can be fixed for models with just one absorber. For the purpose, we reconstruct another dataset of training samples by using new random number. It predicts positions other than the first predicted position. When we use and compare predictions between two sets of detection models, the final accuracy rate reaches 96% as a result of such double classification.

If we employ Gaussian noises, the accuracy rate is much more improved. The model with Gaussian noises can detect the correct position for test data with larger noise of  $\sigma = 0.01$ , which is ten times larger than training data. Using test data with such Gaussian noises, the accuracy rate reaches 100%. If we use a model with uniform random noise of 0.01, then the accuracy rate falls to 89%. It clearly demonstrates that noise types of test data are sensitively recognized by LSTM deep learning. Hereafter we use the detection model based on test data with Gaussian noises.

Also, we study the effects by offsets of absorbers and setups of finer domains. Fig. 4 shows

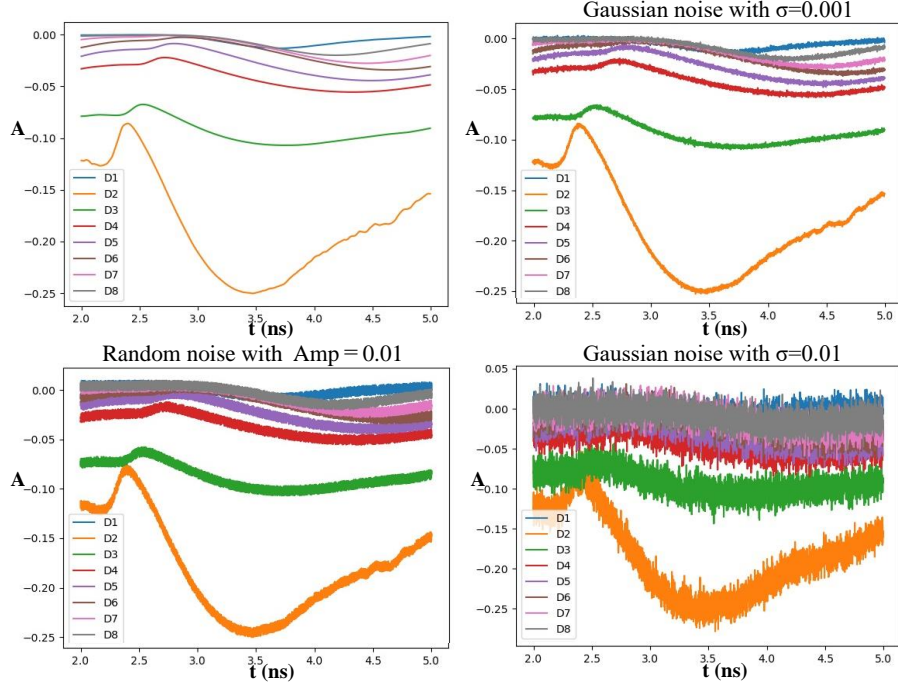


Fig. 3. Generation of datasets with noises: Upper left panel shows raw data by radiative transfer simulations. Lower left panel shows training data for deep learning with uniform random noises whose amplitude is 0.01. Upper right panel shows training data with Gaussian noises whose standard deviation is  $\sigma = 0.001$ , and lower right panel is test data with Gaussian noises of  $\sigma = 0.01$ .

the results for an absorber located between domains. An absorber is shown by a red circle and the predicted position is indicated by a square symbol. The upper left panel shows that the present model can predict a position near the correct position. The upper right panel shows the results for an absorber at the middle of 4 domains. Again, a near position is predicted. Next, we consider the refinement of domains. In the lower panels of Fig. 4, the results for 8 domains are shown. The prediction of a position near the correct position allow us to get more accurate information on the absorber position.

#### 4. Data subtraction method

Here, we demonstrate the effectiveness of data subtraction to detect two absorbers or an absorber bigger than a domain.

##### 4.1. Two absorbers

First, we obtain temporal profiles of absorption measure by radiative transfer calculations for absorbers located at two domains. Then, we apply our model with training data, and make prediction with test data. Once a position of absorber is predicted, we subtract the profile data for the absorber from the original data. Then, we apply again our detection model to the data after subtraction. In this subtraction method, we can successfully predict positions of two absorbers. Fig. 5 shows the results for two absorbers, where orange and green circles are absorbers and predicted positions are indicated by blue squares. In most cases, correct positions or near posi-

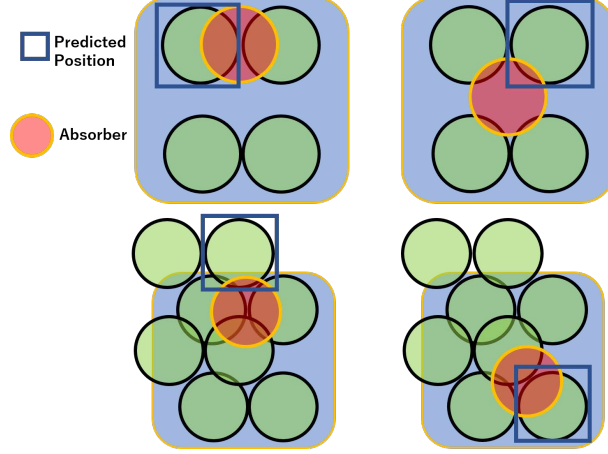


Fig. 4. Results of position prediction for absorbers with offsets. Red circles are absorbers, and blue squares are predicted positions.

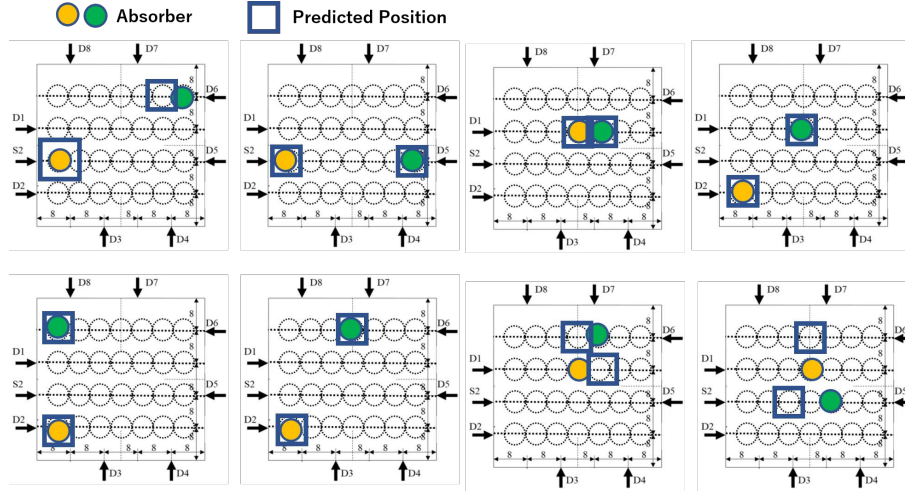


Fig. 5. The results for two absorbers. Orange and green circles are absorbers, and predicted positions are indicated by blue squares.

tions are predicted, while in a lower right case, prediction is not so precise. After we tested 60 cases for two absorbers, we found that the data subtraction method works well to give a high accuracy rate.

These results imply that a linear combination of each absorption profile is a good approximation for most cases of two absorbers. When the distance between two absorbers is long, the linearity makes sense. But, the upper middle panel in the Fig. 5 shows that the linearity is a good approximation even for adjacent absorbers. This is the case where two absorbers are located in parallel to the incident beam direction. However, in the lower right panel, a nonlinear effect by two absorbers seems to be important.



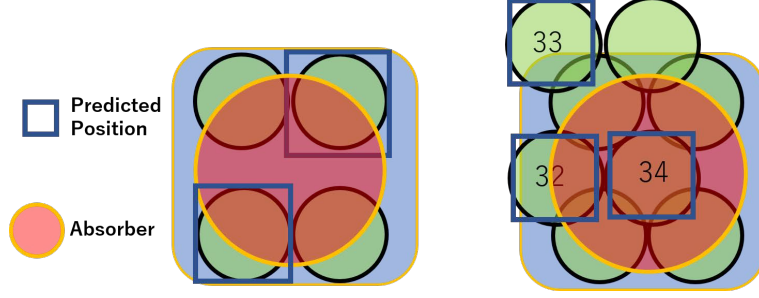


Fig. 6. The results for a big absorber. The left is the classification in 4 domains, while the right is that in 8 domains. A red circle is an absorber, and predicted positions are indicated by blue squares.

#### 4.2. Bigger absorbers

Here, we consider an absorber two times bigger than a domain. Temporal profiles of absorption measure for this absorber is obtained by radiative transfer calculations. Then, our detection method is adopted for the data. Fig. 6 shows the results of prediction for a big absorber. The left panel of Fig. 6 shows the classification based on the subtraction method in 4 domains. Two domains adjacent to the absorbers are predicted with this method. The right panel of Fig. 6 shows the classification in 8 domains. In this case, the machine learning without data subtraction gives us the probability distributions of correct detection. The resultant probabilities for the position: 72% for #34, 16% for #33, and 10% for #32. Such probability distributions are informative for a big absorber. We also suppose the case of 1.5 times bigger absorber, and the resultant probabilities for the position: 75% for #34, 13% for #33, and 8% for #32. Compared to 2 times bigger absorber, probabilities at #32 and #33 are slightly smaller. Thus, these probability distributions reflect the size of absorber.

As shown above, the data subtraction method can predict the correct position or nearest ones. In order to evaluate the probability of correct detection, it is useful to introduce the scoring rule. As shown in the left panel of Fig. 7, the score of correct position is 2, while the score of adjacent positions is 1. The right panel of Fig. 7 shows the example of total scores. If the position of one absorber is correctly predicted, the score is 2, while the score is 1 if an adjacent position of another absorber is predicted. Thus, the total score is 3, which means the detection probability of 75%. Based on the scoring rule, we tested 60 examples for two absorbers and got the detection probability of 72% on average. It means that the most probable prediction for two absorbers is the combination shown in the right panel of Fig. 7, where one absorber is correctly predicted and an adjacent position of another absorber is predicted.

### 5. Multi-beam injection model

So far we considered one incident laser beam from S2 in Fig. 1. Here, we analyze the case where laser beams are injected from multiple positions, that is, S1 to S8 in Fig. 1. We can use 8 datasets for different incident beams. In the data subtraction method, it is found that the detection probability is higher for an absorber located near an incident beam.

Fig. 8 shows the distributions of detection probabilities. In yellow domains that are near the beam position, detection probabilities are high, while probabilities are low in blue domains. If we apply the present method to datasets with Gaussian noises for three incident beams from S1, S2 and S4, the accuracy rate results in 100% to detect one absorber. Also, we tested the multi-beam model for three absorbers, using data subtraction method. The results are shown in



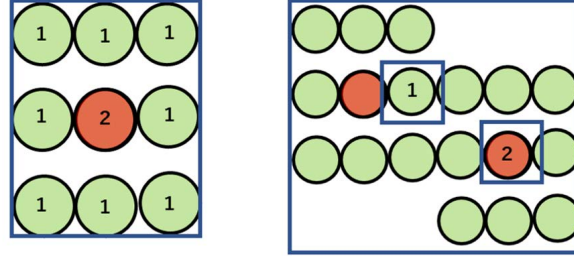


Fig. 7. The left panel shows a point at the position for our scoring. If one detect the absorber position, one get 2 points. The right panel shows one example of scoring for two absorbers, that leads to total 3 points, which means the detection probability of 75%.

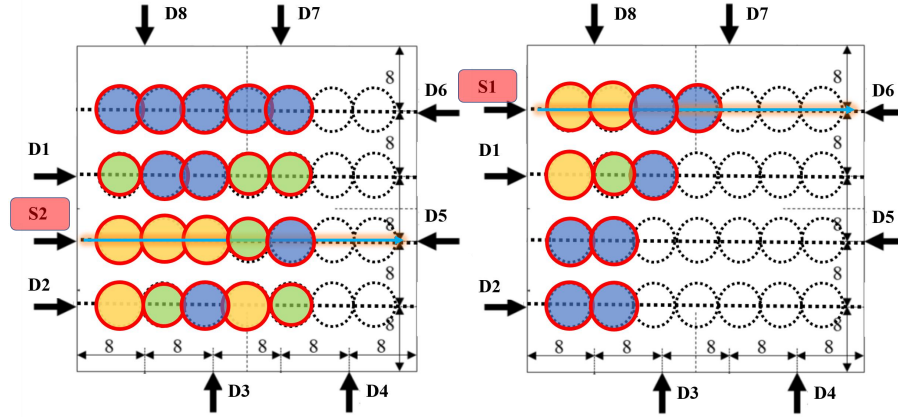


Fig. 8. Distributions of detection probabilities for an incident beam from S2 (left panel) and S1 (right panel): yellow domains are most probable positions for detection, while green domains correspond to medium probabilities and blue domains do to low probabilities.

Fig. 9, where each symbol corresponds to detected positions for each beam. In this example, the blue absorber is correctly detected, while the orange absorber is within two detected positions indicated by squares. The total score is 7, where 4 for S2, 2 for S1 and 1 for S4, to the full score of 12. Hence, this result means accuracy rate of  $7/12 = 58\%$ . If additional datasets are given for different beams, it is expected to improve the accuracy rate for detection.

## 6. Discussion

### 6.1. Validity of 2D RTE

In this paper, we have used 2D simulation data based on a radiation transfer solver TRINITY. Here, we perform 3D Monte Carlo simulations to check the validity of 2D models. We pursue the propagation of  $10^{12}$  photon packets, each of which is injected in random directions from a laser beam point. Each photo packet travels up to its optical depth defined by random number  $R$  as  $\tau = -\log(R)$ . Fig. 10 shows the absorption measure  $A$  calculated by Monte Carlo simulations. Although the profile is quite noisy, it can be integrated over some time interval, that is, a green line in the figure. This feature can be traced by 2D radiative transfer simulations. If we tentatively apply the Monte Carlo simulation data to our machine learning model, we can predict an exact position of absorber.

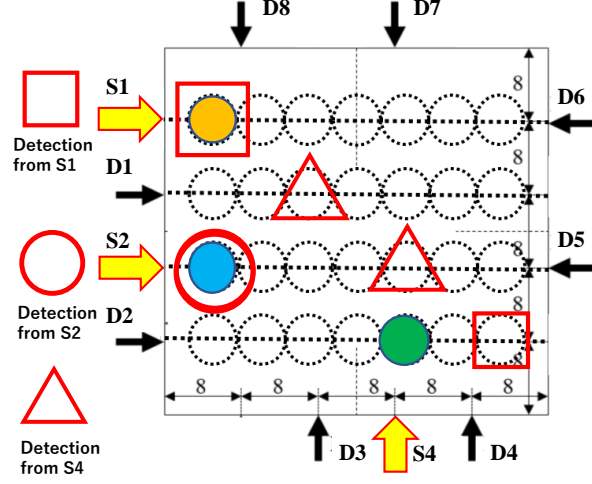


Fig. 9. Example for multi-beam injection model. Three absorbers are located, and three different beams are injected. Each symbol corresponds to detected positions for each beam.

## 6.2. Sampling effect

In the present analyses, we utilized datasets of all time steps for machine learning. Actually, a time step in our simulations is  $\Delta t = 0.0006[\text{ns}]$ , while it is  $\Delta t = 0.01[\text{ns}]$  in experiments using the phantom. One advantage of LSTM deep learning is to recognize global behaviors of temporal data. To check this advantage, we tentatively conducted the same LSTM deep learning using 1/16 data points (16 times longer time steps). As a result, we have confirmed that the present LSTM model does work even for such coarse-grained data. So, this advantage allows us to speed up machine learning dramatically, and to adjust the time step to that of phantom experiments.

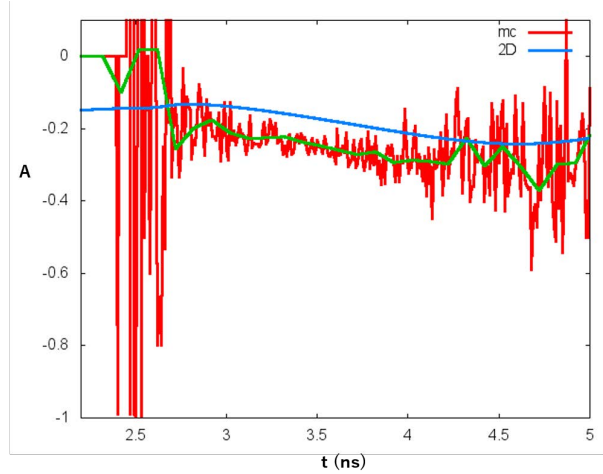


Fig. 10. Absorption measure at the detector D5 calculated by Monte Carlo simulations. A green curve is a smoothed profile of raw data. A blue curve is the result by 2D radiation transfer simulations.

## 7. Summary

In this paper, we have explored a novel deep learning algorithm based on time-domain radiative transfer equation. To specify positions of cancer cells (absorbers), we have applied a long-short-term memory (LSTM) deep learning method to temporal profiles of absorption measure for a two-dimensional model of target tissue, which are calculated by solving time-domain radiative transfer equation.

We have shown that positions of absorbers can be predicted with high accuracy rates by a multi-step classification method. We attempted two types of noises on simulation data and investigated resultant accuracy rates. As a result, we found that LSTM deep learning can recognize sensitively noise types of test data.

We have also developed methods to detect two absorbers or an extended absorber larger than a domain. We demonstrated that data subtraction method successfully works to predict nearly correct positions of absorbers.

The present method is based on the assumption of linear combination of each absorption profile. However, some examples show that nonlinear effects are important. In a future work, we will attempt to extract nonlinear effects to raise the accuracy rate. Also, we tested a multi-beam model for three absorbers and showed the total accuracy rate is 58%. If additional datasets are given for different beams, we expect the accuracy rate of detection can be improved. We will construct a more sophisticated model based on many beams in a future work.

## Acknowledgments

This research is supported by Department of Computational Medical Science in Center for Computational Sciences, University of Tsukuba.

## References

1. Y. Hoshi and Y. Yamada, "Overview of diffuse optical tomography and its clinical applications," *J. Biomed. Opt.* 21(9), 091312 (2016)
2. A. D. Klose, "The forward and inverse problem in tissue optics based on the radiative transfer equation: a brief review," *J. Quant. Spectrosc. Radiat. Transfer* 111(11), 1852-1853 (2010).
3. A. D. Klose, U. Netz, and A. H. Hielscher, "Iterative reconstruction scheme for optical tomography based on the equation of radiative transfer," *Med. Phys.* 26, 1698-1707 (1999).
4. P. González-Rodríguez and A. D. Kim, "Comparison of light scattering models for diffuse optical tomography," *Opt. Express* 17(11), 8756-8774 (2009).
5. L. V. Wang and H.-I. Wu, *Biomedical Optics* (Wiley, 2007).
6. B. W. Pogue, M. Testorf, T. McBride, U. Osterberg, and K. Paulsen, "Instrumentation and design of a frequency-domain diffuse optical tomography imager for breast cancer detection," *Opt. Express* 1(13), 391-403 (1997)
7. S. Okawa, Y. Hoshi, and Y. Yamada, "Improvement of image quality of time-domain diffuse optical tomography with  $l_p$  sparsity regularization," *Biomed Opt. Express* 2(12), 3334-3348 (2011)
8. H. K. Kim and A. H. Hielscher, "A diffusion-transport hybrid method for accelerating optical tomography," *J. Innov. Opt. Health Sci.* 3, 1-13 (2010).
9. T. Tarvainen, V. Kolehmainen, S. R. Arridge, and J. P. Kaipio, "Image reconstruction in diffuse optical tomography using the coupled radiative transport-diffusion model," *J. Quant. Spectrosc. Radiat. Transf.* 112, 2600-2608 (2011).
10. H. Fujii, S. Okawa, Y. Yamada, and Y. Hoshi, "Hybrid model of light propagation in random media based on the time-dependent radiative transfer and diffusion equations," *J. Quant. Spectrosc. Radiat. Transf.* 147, 145-154 (2014)
11. K. Ren, G. Bal, and A. H. Hielscher, "Frequency Domain Optical Tomography Based on the Equation of Radiative Transfer," *SIAM J. Sci. Comput.* 28, 1463-1489 (2006).
12. P. González-Rodríguez and A. D. Kim, "Diffuse optical tomography using the one-way radiative transfer equation," *Biomed. Opt. Express* 6(6), 2006-2021 (2015)
13. J. Yoo, S. Sabir, D. Heo, K. H. Kim, A. Wahab, Y. Choi, S. Lee, E. Y. Chae, H. H. Kim, Y. M. Bae, Y. Choi, S. Cho, and J. C. Ye, "Deep Learning Diffuse Optical Tomography," *IEEE Trans Med Imaging*, 39, 877-887 (2020)
14. I.T. Iliev, and 15 colleagues, "Cosmological radiative transfer codes comparison project - I. The static density field tests", *Monthly Notices of the Royal Astronomical Society* 371, 1057-1086 (2006)